Anaerobic nitrogen cycling on a Neoarchean ocean margin

Mettam, C.[a,b*], Zerkle, A.L.[a], Claire, M.W.[a], Prave, A.R.[a], Poulton, S.W.[c], Junium, C.K.[d]

[a] School of Earth & Environmental Sciences, University of St Andrews, Irvine Building, St Andrews, Fife, KY16 9AL, United Kingdom.

[b] Department of Earth Sciences, University College London, 5 Gower Place, London, WC1E 6BS, United Kingdom (current address).

[c] School of Earth and Environment, University of Leeds, Leeds LS2 9JT, United Kingdom.

[d] Department of Earth Science, Syracuse University, NY 13244-1070, USA.

[*] Corresponding author

Abstract

A persistently aerobic marine nitrogen cycle featuring the biologically mediated oxidation of ammonium to nitrate has likely been in place since the Great Oxidation Event (GOE) some 2.3 billion years ago. Although nitrogen isotope data from some Neoarchaean sediments suggests transient nitrate availability prior to the GOE, these data are open to other interpretations. This is especially so as these data come from deep-water environments that were spatially divorced from shallow-water settings that were the most likely sites for the accumulation of oxygen and the generation of nitrate. Here we present the first nitrogen isotope data from contemporaneous shallow-water sediments to constrain the nitrogen cycle in shallow Late Archean settings. The BH-1 Sacha core through the Campbellrand-Malmani carbonate platform records a transition from a shallow siliciclastic/carbonate ramp to a rimmed carbonate shelf with the potential for reduced communication with the open ocean. In these settings nitrogen isotope ($\delta^{15}N$) data from sub- to peri-tidal and lagoonal settings are close to 0‰, indicating diazotrophy or the complete utilization of remineralised ammonium with an isotopic composition of near 0‰. Our dataset also includes negative $\delta^{15}N$ values that suggest the presence of an ammonium pool of concentrations sufficient to have allowed for non-quantitative assimilation. We suggest that this condition may have been the result of upwelling of phosphorus-rich deep waters into the photic zone, stimulating primary productivity and creating an enhanced flux of organic matter that was subsequently remineralised

and persisted in the dominantly anoxic Neoarchaean marine environment. Notably, we find only limited evidence of coupled nitrification/denitrification, even in these shallow water environments, calling into question previous suggestions that the Late Archean nitrogen cycle was characterized by widespread aerobic nitrogen cycling. Rather, aerobic nitrogen cycling was likely spatially heterogeneous and tied to loci of high oxygen production while zones of shallow water anoxia persisted.

Keywords

- Nitrogen Isotopes
- Carbon Isotopes
- Neoarchean

1. Introduction

Nitrogen (N) is an essential nutrient for the construction of all biomolecules. Despite the biological importance of N_2 and its abundance in the atmosphere, only diazotrophic (N_2-fixing) microbes can directly assimilate di-nitrogen into biomass, which ultimately provides the primary source of nitrogen to the biosphere. In the absence of oxygen, the uptake of ammonium (NH_4^+) from remineralised diazotrophic biomass is the primary source of nitrogen for non-diazotrophs. In oxygen-rich waters, NH_4^+ is rapidly recycled or oxidised by nitrifying microbes to nitrite (NO_2^-) and nitrate (NO_3^-). Nitrate is an important component of dissolved inorganic nitrogen (DIN) in oxygenated waters, and serves as the dominant nitrogen source for primary productivity in modern surface oceans. In such conditions diazotrophic activity will be reduced due to competition with nitrate assimilators for other nutrients (e.g. Sigman et al., 2009).

In low-oxygen settings, such as modern oxygen minimum zones (OMZs), NO_2^- and NO_3^- can also be utilised as electron acceptors in chemotrophic metabolisms. For example, NO_3^- can be used in heterotrophic denitrification or during dissimilatory nitrate reduction to ammonium (DNRA)

(Granger et al., 2008), whilst NO_2^- is utilised in the anaerobic oxidation of ammonium (anammox). Importantly, both annamox and denitrification remove bioavailable nitrogen from the oceanic reservoir and return it to the atmosphere (Cline and Kaplan, 1975), which in extreme cases can lead to nitrate limitation. When bioavailable nitrogen is scarce an expansion of diazotrophy can occur due to reduced competition for nutrients, if other nutrients like Fe or bioactive trace elements are not limiting (Weber and Deutsch, 2013; Sigman et al., 2009).

Due to the redox sensitive nature of these N cycling processes, the global N cycle is believed to have evolved over geologic time alongside changes in the redox state of Earth's oceans and atmosphere (e.g., Stüeken et al., 2016). The 2.33 Ga Great Oxidation Event (GOE) (Luo et al., 2016) marked the time when atmospheric oxygen (O_2) first exceeded 10^{-5} times present atmospheric levels (PAL), as constrained by the disappearance of mass-independent fractionation (MIF) of sulphur isotopes (Farquhar et al., 2011; Pavlov and Kasting, 2002). This change in surface redox conditions seemingly coincided with the widespread expansion of aerobic nitrogen cycling in the world's oceans (e.g., Zerkle et al., 2017; Luo et al., 2018). However, this narrative could be overly simplistic. In particular, small increases of around 2‰ in $\delta^{15}N$ values are preserved in the 2.7-2.5 Ga sediments of the Campbellr and-Malmani carbonate platform from South Africa (Godfrey and Falkowski, 2009), a setting that is spatially and temporally correlated to the sediments analysed in this study, albeit further offshore and a deeper depositional setting. Other positive excursions in $\delta^{15}N$ are reported from studies of Australian Neoarchaean sediments (Garvin et al., 2009; Busigny et al., 2013) and in all settings these nitrogen isotope values have been explained by transient or localized aerobic nitrogen cycling. Alternatively, these small positive shifts in $\delta^{15}N$ values could represent uptake of a residual pool of ^{15}N-enriched ammonium produced by partial nitrification or partial assimilation, or by nitrogen redox cycling independent of environmental oxygenation (e.g., Thomazo et al., 2011; Busigny et al., 2013; Ader et al., 2016). However, there are currently no $\delta^{15}N$ records of contemporaneous shallow-water sediments available to distinguish between these alternatives.

78 Here, we investigate $\delta^{15}N$ values preserved in shallow-water sediments from the 2.7-2.5 Ga
79 Campbellrand-Malmani carbonate platform. These sediments, from the BH-1 Sacha core, represent
80 the shallow-water equivalent to previously investigated deeper-water sediments (GKP01 core;
81 Fischer et al., 2009), in which $\delta^{15}N$ values rose by about 2‰ and were interpreted to represent
82 transient aerobic nitrogen cycling (Godfrey and Falkowski, 2009). If aerobic nitrogen cycling was
83 even intermittently pervasive in this basin, we would expect sediments from these shallower water
84 settings to record similar $\delta^{15}N$ values to deeper-water sediments, particularly given their potential
85 proximity to surface ocean oxygen oases, as shown by the presence of microbial sedimentary
86 structures (Altermann and Siegfried, 1997).

87 **2. Tracking the nitrogen cycle through time**

88 Transformations in the marine nitrogen cycle can modify nitrogen isotope signals ($^{15}N/^{14}N$; $\delta^{15}N$ (‰)
89 = $(((^{15}N/^{14}N)_{sample} /(^{15}N/^{14}N)_{air} – 1) \times 1000)$, leading to fractionation effects between the reactants and
90 products (Casciotti, 2009; Sigman et al., 2009; Zerkle et al., 2008; Brunner et al., 2013; Möbius, 2013;
91 Zhang et al., 2014; McCready et al., 1983; Ader et al., 2016). However, in modern settings, most
92 nitrogen assimilation or redox transformations utilise all available substrates, leading to no apparent
93 fractionation effects (Sigman et al., 2009). The exceptions are diazotrophy and nitrate/nitrite-
94 reduction processes, including denitrification, DNRA, and anammox. Diazotrophy generally produces
95 biomass with $\delta^{15}N$ values between ~+1 and ~–1‰ (Zhang et al., 2014; Bauersachs et al., 2009),
96 although extreme values as low as ~–4‰ have been experimentally demonstrated (e.g., as reviewed
97 in Zerkle et al., 2008). The contribution of diazotrophy to total biomass in modern ocean settings is
98 limited except under oligotrophic conditions, as NO_3^- and NH_4^+ assimilators compete more
99 successfully for other nutrients (Weber and Deutsch, 2013). However, in most oxygen-rich settings,
100 NH_4^+ sourced from remineralised biomass is rapidly oxidized, such that nitrate is the main form of
101 nutrient N. In the modern ocean incomplete denitrification in the water column renders this pool of

bioavailable ^{15}N-enriched , leading to marine organic matter (OM) with an average $\delta^{15}N$ of +5 ‰ to +6‰ (Peters et al., 1978; Sigman et al., 2003; Galbraith et al., 2013).

The $\delta^{15}N$ of marine biomass thus records the dominant forms of bioavailable nitrogen utilised for primary productivity, particularly on a local scale. These signals are ultimately archived in sedimentary rocks, either directly in OM or retained as mineral-associated nitrogen derived from degraded OM (e.g., Stüeken et al., 2016; Freudenthal et al., 1999). Variations in the $\delta^{15}N$ of sedimentary rocks can thus be utilized to track changes in the marine nitrogen cycle through geological time.

3. Geological setting

The Campbellrand-Malmani Platform in South Africa (Fig. 1A, B and C) is part of the Transvaal Supergroup. A ~3,700 m section of these rocks was recovered in the BH1-Sacha core and logged in detail by Altermann and Siegfried (1997). The lowermost recovered strata are a succession of interbedded doloarenites, quartzites, and shales with microbial laminites from the top of the Vryburg Formation (Fm) (Altermann and Siegfried, 1997). Thick (> 10 m) shale beds in the lower part of the core likely represent deeper shelf conditions when marine transgressions mark the beginning of several deepening and shallowing cycles, with carbonates likely representative of the shallowest regressive conditions. Thin (< 10 m) shales interbedded with carbonates throughout the core are mostly likely evidence of slightly deeper lagoonal conditions during generally regressive periods (Altermann and Siegfried, 1997). A major flooding surface defines the base of the overlying Boomplaas Fm, but its top is defined by an oolite bed indicating shallow, wave-agitated conditions. The Lokammona Fm is marked by several, variably developed, shoaling cycles similar to those in the Vryburg Fm (Sumner and Beukes, 2006). These three formations comprise the Schmidtsdrift Subgroup, and are overlain by the Monteville Fm of the lowermost Campbellrand Subgroup, which shows cycles similar to the Lokammona Fm (Sumner and Beukes, 2006). Together, these four

126 formations are interpreted as representing deposition of sediments on an evolving ramp structure
127 (Fig. 1B).

128 From the Reivilo Fm upwards, depositional conditions are considered to have been generally
129 shallow, with subtidal, intertidal or lagoonal conditions dominating as inferred from the presence of
130 domal, columnar, elongate and small, bifurcating, finger-like stromatolites, birds-eye structures, flat-
131 pebble breccias and chert beds (Altermann and Siegfried, 1997; Sumner and Beukes, 2006; Fischer
132 and Knoll, 2009). These facies are considered to represent the replacement of ramp-like conditions
133 with a rimmed-, carbonate-dominated shallow-shelf, platform-top (Sumner and Grotzinger, 2004;
134 Sumner and Beukes 2006). A maximum metamorphic grade of sub-greenschist is reported for the
135 section of the Campbellrand-Malmani Platform studied here (Button, 1973; Miyano and Beukes,
136 1984; Fischer et al., 2009), consistent with minimal alteration of stable isotope values as indicated by
137 our data (see discussion below). A U-Pb zircon age of 2,714 ± 8 Ma from the underlying Ventersdorp
138 Supergroup provides a maximum age for the Campbellrand-Malmani Platform (Armstrong et al.,
139 1991) and tuffs within the Schmidtsdrift and Campbellrand subgroups have yielded stratigraphically
140 coherent Neoarchaean ages (Barton et al., 1995; Walraven and Martini, 1995; Fischer et al., 2009;
141 Knoll and Beukes, 2009; ranges of published dates are in the supplementary material).

142 **4. Methods**

143 Samples were collected from the National Core Repository at Donkerhoek (Pretoria, South Africa).
144 Sampling was predominantly focussed on black shales, which were anticipated to have high-TOC
145 content. Samples were ground into homogenous powders in agate ball mills, and carbonate was
146 removed via two 24 hour digestions in 10 % (vol/vol) HCl. After each digestion the samples were
147 centrifuged and the supernatant was discarded and replaced with fresh 10% HCl. Sample residues
148 were washed until pH neutral using ultrapure water (18.2 MΩ•cm) and dried at < 40 °C. Carbonate
149 content was calculated gravimetrically from dry sample residues which were then homogenised
150 using an agate pestle and mortar and stored in glass vials. Several samples of mid-grey carbonate

rocks, assumed to contain some OM, were also decarbonated to assess the possibility of extracting kerogen. This method of carbonate abundance determination is prone to inaccuracy. However, here it is used only to provide a broad assessment of lithological characteristics, for example between rocks with high carbonate content (e.g. > 85%), and those with low carbonate concentrations (e.g. <10%). Kerogen was extracted at the University of St Andrews by digestion of decarbonated residues in HF/HCl following established protocols (e.g., Zerkle et al., 2017).

Nitrogen isotope values for kerogen ($\delta^{15}N_{org}$) and decarbonated sediments ($\delta^{15}N_{bulk}$) were determined by nano-EA-IRMS in the GAPP Lab at Syracuse University, USA. Prior to analyses, samples and standards were placed into a vacuum chamber overnight to remove atmospheric nitrogen and flooded with Argon (Ar) prior to analysis. Upon introduction into the EA, tin capsule sealed samples were further purged with helium (He) for 45 seconds prior to combustion in an Elementar Vario Isotope Cube coupled to a Trace Gas analyser. Oxidation and reduction reactor temperatures were 1100 ^{o}C and 650 ^{o}C, respectively. Helium carrier gas flow was 150 ml/min; and the O_2 pulse was set for 90 seconds. Resultant sample gas was trapped in a liquid-N silica gel filled cryotrap, before release to an Elementar Isoprime 100 IRMS via an Agilent CarboBond capillary column (25 m x 0.53 mm x 5 um) with a He flow rate of ~2 cm^3 min^{-1} (e.g., Polissar et al., 2008; Zerkle et al., 2017; Luo et al., 2018). Data accuracy for $\delta^{15}N_{org}$ was assessed using the IAEA N1 (Ammonium Sulphate, $(NH_4)_2$ SO_4) standard which provided a mean $\delta^{15}N$ value of 0.11± 0.50‰ (1σ; n=30) versus a certified value of +0.40 ± 0.2‰ (1σ).

The extremely sensitive nature of the nano-EA-IRMS method generates relatively large peak height sizes for the blank, in comparison to standard IRMS techniques. This, coupled with relatively nitrogen-poor kerogen samples, led to blank-sample ratios that could introduce variability in $\delta^{15}N_{org}$ measurements. Blank-corrected $\delta^{15}N_{org}$ were calculated by blank extraction using the following equation:

175 $$\delta^{15}\mathrm{N}_{\mathrm{org}} = \frac{\left(\mathrm{Peak\ Area}_{\mathrm{sample}} * \delta^{15}\mathrm{N}_{\mathrm{sample}}\right) - \left(\mathrm{Peak\ Area}_{\mathrm{blank}} * \delta^{15}\mathrm{N}_{\mathrm{blank}}\right)}{\left(\mathrm{Peak\ Area}_{\mathrm{sample}} - \mathrm{Peak\ Area}_{\mathrm{blank}}\right)}$$

176 The size $(\mathrm{Peak\ Area}_{\mathrm{blank}})$ and isotopic composition of the blank $(\delta^{15}\mathrm{N}_{\mathrm{blank}})$ contribution to each
177 sample measurement was calculated by measuring a blank (without tin cup) before and after each
178 five samples and calculating incremental change for both values between the two blanks. This
179 method was also applied to blank corrections for the standard IAEA N1 and provided robust blank
180 corrections. Duplicates of sample BH1-330, corrected to IAEA N1 indicate reproducibility of $\delta^{15}N_{org}$
181 was ± 0.02‰ (1σ), whilst triplicates of samples BH1-1963 and BH1-3144.33 produced values ±
182 0.49‰ (1σ) and ± 0.32‰ (1σ), respectively. Duplicates of samples with large blank contributions
183 resulting from exceptionally low N_{org} produced higher variability, resulting in $\delta^{15}N_{org}$ measurements
184 on samples below 0.05 wt. % N being discarded. Error bars for $\delta^{15}N_{org}$ plots were calculated using
185 standard deviation of triplicates (BH1-1963.6; 0.49‰) and standard deviation of standards (0.50‰;
186 n=30), where error bar = √ (error of standards^2 + largest error of corrected sample^2)].

187 Decarbonated sediments were also analysed to measure $\delta^{15}N_{bulk}$ values. Again, nitrogen abundances
188 in these decarbonated residues (TN_{bulk}) were exceptionally low, ranging from 0.0018 wt. % to 0.017
189 wt. %, so samples were run in triplicate and $\delta^{15}N_{bulk}$ values determined by Keeling plots. These
190 samples were corrected to the reference material NIST1547 – Peach Leaves, which returned a $\delta^{15}N$
191 value of +1.76‰ (n=8, determined by Keeling plots) against a certified value of +1.98‰ for
192 measurement of triplicate samples and +2.10‰ (n=5) for sample 3364 reruns (Table S4). Error bars
193 for $\delta^{15}N_{bulk}$ reflect the combined standard deviation of standards and the intercept errors of keeling
194 plots for each individual sample triplicate using the same formula. These individual errors are shown
195 in supplementary table four.

196 Organic carbon isotope values ($\delta^{13}C_{org}$) for this study were measured at the University of St Andrews
197 via flash-combustion of decarbonated residues using a Costech 4010 EA equipped with a zero blank
198 autosampler and interfaced with a Thermo Finnigan Delta Plus XP IRMS in continuous flow mode.

Data accuracy was verified using an internal standard (n=5), and returned values of -25.07 ± 0.18‰ (1σ) and -25.05 ± 0.11‰ (1σ) against an accepted value of -25.04‰. Nitrogen and carbon isotope values are reported using the standard delta notation showing per mil deviations from V-PDB for $\delta^{13}C$, and relative to N_{air} for $\delta^{15}N$.

The abundance of nitrogen in kerogen (N_{org}) and in decarbonated residues (TN_{bulk}) and the total organic carbon content (TOC) of whole rock powders were calculated by comparing peak areas generated during isotope analyses with those of standards with known abundances (Table S3 and S4). To calculate TOC abundances, the carbon yield was adjusted according to the mass lost during decarbonation.

Potassium (K) and iron (Fe) abundances for samples 2709 and 3364 were determined by XRF at Department of Earth and Environment, Franklin and Marshall College, USA. Standards returned 0.51 wt. % ±0.0014 (1σ) against a certified value of 0.52 wt. % for K_2O and 12.42 wt. % ±0.0135 (1σ) against a certified value of 12.30 wt. % for Fe_2O_3. Data for the remaining four samples were analysed at University of St Andrews using standard XRF providing a standard deviation of 1σ of 0.02 wt. % for K_2O.

5. Results

Nitrogen isotope values from kerogen ($\delta^{15}N_{org}$) for BH1-Sacha (Fig. 2; Table 1) range from –2.73‰ to +3.18‰ (mean –0.23 ± 1.59‰ here and elsewhere, 1σ, n=21). With the exception of samples BH1-3113.32 and BH1- 3144.33, all $\delta^{15}N_{org}$ values of greater than 0‰ are from samples with carbonate abundance in excess of 85% (Fig. 2; Table S1). Bulk nitrogen isotope values ($\delta^{15}N_{bulk}$) range from –3.30‰ to +2.94‰ (mean +0.58 ± 2.14‰, n=6). Organic carbon isotope values ($\delta^{13}C_{org}$) for BH1-Sacha (Fig. 2; Table S1, including a subset from Izon et al. [2015]) range from –46.09‰ to –27.36‰ (mean –36.69 ± 3.76‰, n=26).

For data binned by depositional setting, the ramp-top settings of the Schmidsdrift Subgroup and overlying Monteville Fm have mean $\delta^{15}N_{bulk}$ values of +0.11 ± 2.01‰ (n=5) and $\delta^{15}N_{org}$ values of +0.22 ± 1.96‰, n=7 (Fig. 2; Table S1). The highest $\delta^{15}N_{org}$ values measured are from two carbonate-rich facies: +2.48‰ at 3306.3 m core depth, and +3.18‰ at 3114.5 m. The highest and lowest $\delta^{15}N_{org}$ values from siliciclastic facies in this section are +0.53‰ and –2.03‰, whilst $\delta^{15}N_{bulk}$ values range from –3.30‰ to +2.02‰. Mean $\delta^{13}C_{org}$ values from these ramp depositional settings are –34.27 ± 3.63‰, n=11.

In the platform- top/ rimmed-shelf facies from the base of the Reivilo Fm through the Gamohaan Fm, the mean $\delta^{15}N_{org}$ values are –0.52± 1.36‰ (n=15) with a single $\delta^{15}N_{bulk}$ value of +2.94‰ (Fig. 2; Table S1). Again, the three carbonate samples had significantly higher $\delta^{15}N$ values, up to +3.17‰. Mean $\delta^{13}C_{org}$ values for these facies are –38.13 ± 3.26‰ (n=15).

6. Discussion

6.1. Preservation of Primary Isotopic Signals

Diagenetic and metamorphic processes can produce changes in primary carbon and nitrogen isotope values, generally driving $\delta^{13}C_{org}$ and $\delta^{15}N$ values heavier and/or causing a divergence between bulk rock and kerogen $\delta^{15}N$. At the sub-greenschist facies conditions of the Campbellrand-Malmani Platform (Button, 1973; Miyano and Beukes, 1984; Fischer et al., 2009) such effects should be minimal, and not exceed 1 – 2‰ (Stüeken et al., 2017). However, we examined trends in stable isotope values alongside elemental abundances to evaluate possible contributions from post-depositional alteration.

Thermal maturation during diagenetic or metamorphic processes can preferentially remove ^{12}C and ^{14}N from sediments, leading to diagnostic positive correlations between $\delta^{15}N_{bulk}$ and $\delta^{13}C_{org}$, and negative correlations between the abundances of TOC and $\delta^{13}C_{org}$, the abundances of TN_{org} and $\delta^{15}N_{org}$, and the abundances of TN_{bulk} and $\delta^{15}N_{bulk}$. We note a weak positive correlation between TN_{org}

and $\delta^{15}N_{org}$ (R^2 = 0.28; Fig. 3A) and a moderately positive correlation between TN_{bulk} and $\delta^{15}N_{bulk}$ (R^2 = 0.51; Fig. 3E). We also note a weak positive correlation between $\delta^{15}N_{org}$ and $\delta^{13}C_{org}$ (R^2 = 0.24; Fig. 3B) and a weak negative correlation between TOC/TN_{org} and $\delta^{15}N_{org}$ (R^2 = 0.37, Fig. 3C). We note no correlation between TOC and $\delta^{13}C_{org}$ (R^2 = 0.10; Fig. 3D), and no correlation between $\delta^{15}N_{bulk}$ and $\delta^{13}C_{org}$ (R^2 = 0.05; Fig. 3F). Therefore, our data show little evidence for significant post-depositional alteration of $\delta^{13}C_{org}$ or $\delta^{15}N$, consistent with the low metamorphic grade of these sediments. We also examine the potential influence of nitrogen adsorbed onto detrital clays by comparing potassium (K) content with TN_{bulk} and $\delta^{15}N_{bulk}$ (Figs. 3G and H).

We do note that there is a moderate correlation (R^2 = 0.69) between K and $\delta^{15}N_{bulk}$ suggesting that higher concentrations of clay-bound ammonium could be associated with more-positive $\delta^{15}N_{bulk}$ values, although, this correlation is somewhat influenced by the one sample in this small data set. The sample from 3364m is unusual in that negative (-3.3‰) $\delta^{15}N_{bulk}$ values are associated with very low K abundances (0.97%) in comparison to the remaining samples (Table S6). When this sample is removed from the analyses the correlation between K and $\delta^{15}N_{bulk}$ is more modest (R^2 = 0.32) which more closely reflects the very limited correlation (R^2 = 0.17) between TN_{bulk} and K abundances.

6.2. Nitrogen cycling in a marginal marine environment

The majority of samples analysed in this study are from relatively thin shale units that were intercalated with stromatolitic carbonates. These thin shales are interpreted to have been deposited during small marine transgressions, overprinted upon longer-term, relatively shallow, potentially lagoonal conditions in platform and ramp-top settings (Altermann and Siegfried, 1997; Sumner and Beukes, 2006; Ergolu et al., 2017). These thin shales are distinct from thicker shale units that likely represent more open and deeper marine settings. Given the shallow nature of this setting and the presence of microbial mats within the photic zone, such conditions should be prime candidates for pre-GOE oxygen oases. Although the persistence of sulphur MIF in the BH-1 Sacha record indicates that atmospheric oxygen concentrations must have remained less than 1 ppm during this time (Izon

et al., 2015), oxygen concentrations could have been sufficiently high in the water column or locally associated with benthic microbial mats to allow for aerobic biogeochemical cycling. Indeed, trace element and iron speciation analyses from Neoarchaean sediments of the Campbellrand-Malmani Platform suggest a stratified ocean with mildly oxygenated surface oxygen oases (Kendall et al., 2010; Czaja et al., 2012; Eroglu et al., 2015) and localized oxygen production in microbial mats (Zerkle et al., 2012). Previous studies of trends in $\delta^{15}N$ from deeper water sediments from this basin have also been interpreted to represent transient aerobic N cycling (Godfrey and Falkowski, 2009).

We find that $\delta^{15}N_{org}$ values from siliciclastic sediments deposited in these near-shore settings are inconsistent with widespread coupled nitrification /denitrification. In particular, $\delta^{15}N$ values close to 0‰ are more consistent with a nitrogen cycle dominated by diazotrophy and the recycling of NH_4^+, and suggest that any NO_3^- generated from localized oxidation of ammonium was quantitatively and rapidly removed by denitrification and anammox. Even if NO_3^- was present, it likely provided a secondary nutrient N source given that ammonium could have been persistently available under widely anoxic water column conditions. In modern settings (e.g., Higgins et al., 2012) cyanobacteria can assimilate both NH_4^+ and NO_3^- as a source of nitrogen, and it has been noted that genes controlling the assimilation of oxidised nitrogen sources can be repressed in the presence of ammonium (Flores et al., 2005).

The lower part of the BH1-Sacha core (e.g., the Schmidsdrift Subgroup and Monteville Fm) represents depositional conditions that were likely open to the ocean. Both $\delta^{15}N_{bulk}$ and $\delta^{15}N_{org}$ values in these ramp facies (with the exception of samples at 3114.5m and 3306.3m, discussed below) are again consistent with anaerobic nitrogen cycling. Intriguingly, one sample (3364m) provided a $\delta^{15}N_{bulk}$ value of –3.3‰, and another sample (3125.05m) a $\delta^{15}N_{org}$ value of -2.0‰, showing greater ^{15}N depletion than biomass generally produced by modern marine diazotrophs. This is especially the case when considering that the long-term diagenetic or metamorphic effects could possibly have elevated $\delta^{15}N$ by a few per mille in comparison to the $\delta^{15}N$ of primary organic matter.

We suggest that these strongly negative $\delta^{15}N$ values indicate the generation of biomass from partial assimilation of NH_4^+, as recently suggested for ~2.7 Ga sediments (Yang et al., 2019). Ammonium could have accumulated in deep waters under upwelling zones that supported high rates of diazotrophic productivity and organic matter export (Fig. 4A, B). The remineralisation of this organic matter at depth under anoxic conditions could have led to the formation of a deep-water NH_4^+ pool. In turn, these ammonium-rich waters could have been upwelled, leading to partial NH_4^+ assimilation by primary producers, thus forming ^{15}N-depleted organic matter. Such settings could have included the ramp front during early platform formation (e.g., thicker shale units at 3364m) and later the mature platform front (the latter a depositional setting not recorded in the BH1-Sacha core), both of which represented relatively deeper conditions in contrast to shallow lagoonal depositional settings. Other negative $\delta^{15}N$ values (e.g., those associated with thin shales intercalated with carbonates) could represent times when communication between the lagoonal setting and the open ocean was more vigorous and allowed NH_4^+-rich deep waters to temporarily inundate the lagoon.

Sediments at 3364m have high Fe concentrations (14.8%; Table S6) that approach the lower boundary of Fe abundances in banded iron formations, despite being deposited in open-ramp conditions. It is possible that in these Fe-rich conditions, diazotrophs utilizing the FeMo nitrogenase enzyme produced biomass with $\delta^{15}N$ values down to -4‰, similar to those reported in Zerkle et al. (2008). In addition, diazotrophs using alternative nitrogenase enzymes (e.g., Fe-Fe or Fe-V) have been shown to produced biomass with $\delta^{15}N$ values down to -7‰ when Mo is limited (Zhang et al., 2014). However, large variations in $\delta^{98}Mo$ have been reported for the lower Campbellrand-Malmani Platform, which provide evidence for a sizeable Mo reservoir (Eroglu et al., 2015). It is therefore unlikely that diazotrophs would have relied on these less efficient alternative enzymes in this environment.

Such low $\delta^{15}N$ values are unusual, but not unreported in modern oceans and in the more recent geologic past (e.g. Higgins et al., 2012). For example, $\delta^{15}N$ values of ~–5‰ have been reported for

particulate nitrogen, and attributed to the partial utilization of ammonium (Rau et al., 1991) and nitrate (Altabet and Francois, 1994). In the latter case, these low values are associated with incomplete utilisation of nitrate in seasonally upwelling waters. However, this degree of ^{15}N-depletion is not recorded in subsequent sedimentary $\delta^{15}N$ values due to the integration of multiple seasonal signals representing different rates of nitrate utilisation. The fact that some low $\delta^{15}N$ values are recorded in the Neoarchaean sediments studied here suggests that ammonium had accumulated to significant levels to remain under-utilised and that nitrogen limitation was not a significant factor in the wider oceans.

Intriguingly, widespread partial assimilation of ammonium could have left the residual pool of NH_4^+ relatively ^{15}N-enriched (e.g., Yang et al., 2019). If transported offshore, uptake from a pool of heavier NH_4^+ could generate ^{15}N-enriched organic matter in more distal ocean settings (Fig. 4A, B; e.g., Busigny et al., 2013). This was illustrated numerically by Yang et al. (2019) using a simple Rayleigh model based on the experimental calibrations of isotope effects during ammonium uptake (Hoch et al., 1992). This scenario provides an alternative explanation for the presence of positive $\delta^{15}N$ values recorded in relatively distal Neoarchaean settings in the Griqualand West Basin (e.g., Godfrey and Falkowski, 2009).

The majority of our $\delta^{15}N$ data point to a largely anaerobic marine N cycle, driven by N_2 fixation and varying degrees of ammonium uptake and recycling. However, a handful of carbonate-rich facies show positive $\delta^{15}N_{org}$ values outside the range of typical values for N_2 fixation (up to +3.2‰; Fig. 4, Table S1). Elevated $\delta^{15}N$ values could indicate syn-depositional oxidative degradation (Freudenthal et al., 2001; Möbius et al., 2010). However, these $\delta^{15}N_{org}$ values could hint at the potential influence of nitrification and incomplete denitrification in localised, mildly-oxygenated settings during the deposition of carbonates, potentially periods when waters were likely shallower than when thin muds were deposited. Ergolu et al. (2017) have argued that large differences in $\delta^{13}C_{org}$ values between carbonates and mudstones in the shallower parts of the Campbellrand-Malmani Platform

were due to different consortia of microbes that comprise microbial mats in the two settings. They suggested that during the deposition of carbonates, microbial mats could have had larger proportions of oxygenic photoautotroph than during the deposition of mudrocks, with anaerobic microbes more prevalent during the deposition of the latter. This scenario could support shallow microbial mat communities as epicentres of highly localised nitrification-denitrification, without a major role for aerobic N cycling in the Late Archean.

6. Conclusions

Here we describe the Neoarchean nitrogen cycle in a shallow marginal marine setting, during the evolution of a well-defined carbonate platform into a relatively isolated platform- top/ rimmed-shelf lagoonal environment. Nitrogen isotope values range from -3.3 to +3.2‰ and are consistent with a predominantly anaerobic nitrogen cycle, dominated by N_2 fixation and the assimilation and recycling of upwelling NH_4^+. Evidence for the presence of oxidised nitrogen species is limited, suggesting that any NO_3^- generated during periods of transient oxygen availability was quantitatively removed by anaerobic respiration. However, rare $\delta^{15}N$ values > 0 ‰ recorded in carbonate-rich sediments hint at highly localized areas of nitrification and partial denitrification. In addition, the inclusion of some very light $\delta^{15}N$ values suggest partial assimilation of an upwelling pool of ammonium, leaving a residual pool of ^{15}N-enriched NH_4^+ that could potentially explain small increases in $\delta^{15}N$ from contemporaneous open-ocean settings. We thus conclude that N cycling in the shore-proximal marine environment of the Griqualand West basin was controlled by anaerobic processes and recycling of bioavailable nitrogen, and that nitrification/denitrification was unlikely to have been widespread prior to the end of the Neoarchaean.

Acknowledgements

This study was supported financially by NERC Fellowship NE/H016805/2 (to AZ), NERC Standard Grant NE/J023485/2 (to AZ and MC), NSF EAR-1455258 (to CKJ).

370 **References**

371 Ader, M., Thomazo, C., Sansjofre, P., Busigny, V., Papineau, D., Laffont, R., Cartigny, P., Halverson,
372 G.P., 2016. Interpretation of the nitrogen isotopic composition of Precambrian sedimentary rocks:
373 Assumptions and perspectives. *Chem. Geol.* 429, 93 - 110.

374 Altabet, M.A., 1988. Variations in nitrogen isotopic composition between sinking and suspended
375 particles: Implications for nitrogen cycling and particle transformation in the open ocean. *Deep Sea*
376 *Res. A*. 35, 535 – 554.

377 Altabet, M.A., Francois, R., 1994. Sedimentary nitrogen isotopic ratio as a recorder for surface ocean
378 nitrate utilization. *Global biogeochemical cycles* 8, 103 – 116.

379 Altermann, W., Siegfried, H.P., 1997. Sedimentology and facies development of an Archaean shelf:
380 carbonate platform transition in the Kaapvaal Craton, as deduced from a deep borehole at Kathu,
381 South Africa. *J. Afr. Earth Sci.,* 24, 391 - 410.

382 Armstrong, R.A., Compston, W., Retief, E.A., Williams, I.S., Welke, H.J., 1991. Zircon ion microprobe
383 studies bearing on the age and evolution of the Witwatersrand triad. *Precamb. Res*. 53, 243 - 266.

384 Barton, J.M.J., Blignaut, E., Salnikova, E.B., Kotov, A.B., 1995. The stratigraphical position of the
385 Buffelsfontein Group based on field relationships and chemical and geochronological data. *S. Afr. J.*
386 *of Geol*. 98, 386 - 392.

387 Bauersachs, T., Schouten, S., Compaoré, J., Wollenzien, U., Stal, L.J., Damsteé, J.S.S., 2009. Nitrogen
388 isotopic fractionation associated with growth on dinitrogen gas and nitrate by cyanobacteria. *Limnol.*
389 *Oceanogr.* 5, 1403 - 1411.

390 Brunner, B., Contreras, S., Lehmann, M.F., Matantseva, O., Rollog, M., Kalvelage, T., Klockgether, G.,
391 Lavik, G., Jetten, M.S.M., Kartal, B., Kuypers M.M., 2013. Nitrogen isotope effects induced by
392 anammox bacteria. *P.N.A.S.* 110, 18994 - 18999.

Busigny, V., Lebeau, O., Ader, M., Krapez, B., Bekker, A., 2013. Nitrogen cycle in the Late Archean ferruginous ocean. *Chem. Geol.* 362, 115 - 130.

Button, A., 1973. The stratigraphic history of the Malmani dolomite in the eastern and north-eastern Transvaal. *Verh. Geol. Ver. S.-Afr*. 76, 229 - 247.

Casciotti, K.L. 2009. Inverse kinetic isotope fractionation during bacterial nitrite oxidation. *Geochim. Cosmochim. Acta.* 73, 2061 - 2076.

Cline, J.D., Kaplan I.R., 1975. Isotopic fractionation of dissolved nitrate during denitrification in the eastern tropical north Pacific Ocean. *Marine Chem*. 3, 271 - 299.

Czaja, A.D., Johnson, C.M., Roden, E.E., Beard, B.L., Voegelin, A.R., Nägler, T.F., Beukes, N.J., Wille, M., 2012. Evidence for free oxygen in the Neoarchean ocean based on coupled iron–molybdenum isotope fractionation. *Geochim. Cosmochim. Acta.* 86, 118 - 137.

Eroglu, S., Schoenberg, R., Wille, M., Beukes, N., Taubald, H., 2015. Geochemical stratigraphy, sedimentology, and Mo isotope systematics of the ca. 2.58–2.50 Ga-old Transvaal Supergroup carbonate platform, South Africa. *Precamb. Res*. 266, 27 - 46.

Eroglu, S. van Zuilen, M.A., Taubald, H., Drost, K., Wille, M., Swanner, E.D., Beukes, N.J., Schoenberg, R., 2017. Depth-dependent $\delta^{13}C$ trends in platform and slope settings of the Campbellrand-Malmani carbonate platform and possible implications for Early Earth oxygenation. *Precamb. Res.* 302, 122 - 139.

Farquhar, J., Zerkle, A.L., Bekker, A., 2011. Geological constraints on the origin of oxygenic photosynthesis. *Photosynth. Res.* 107, 11 - 36.

Fischer, W.W., Schroeder, S., Lacassie, J.P., Beukes, N.J., Goldberg, T., Strauss, H., Horstmann, U.E., Schrag, D.P., Knoll, A.H., 2009. Isotopic constraints on the Late Archean carbon cycle from the

415 Transvaal Supergroup along the western margin of the Kaapvaal Craton, South Africa. *Precambrian*
416 *Res.* 169 15 - 27.

417 Fischer, W.W., Knoll, A.H., 2009. An iron shuttle for deep water silica in Late Archean and early
418 Paleoproterozoic iron formation. *G.S.A. Bull.* 121, 222 - 235.

419 Flores, E., Frías, J.E., Rubio, L.M., Herrero, A., 2005. Photosynthetic nitrate assimilation in
420 cyanobacteria. *Photosynth. Res.* 83: 117 – 133.

421 Freudenthal, T., Wagner, T., Weinzhöffer, F., Zabel, M., Wefer, G., 2001. Early diagenesis of organic
422 matter from sediments of the eastern subtropical Atlantic: Evidence from stable nitrogen and carbon
423 isotopes. *Geochim. Cosmochim. Acta*. 65, 1795 - 1808.

424 Galbraith, E.D., Kienast, M., & The NICOPP working group members, 2013. The acceleration of
425 oceanic denitrification during deglacial warming. *Nat. Geosci*. 6, 579 - 584.

426 Garvin, J., Buick, R., Anbar, A.D., Arnold, G.L., Kaufman, A.J., 2002. Isotopic evidence for an aerobic
427 nitrogen cycle in the latest Archean. *Science.* 323, 1045 - 1048.

428 Godfrey, L.V., Falkowski, P.G., 2009. The cycling and redox state of nitrogen in the Archaean ocean.
429 *Nat. Geosci.* 2, 735 - 729.

430 Granger, J., Sigman, D.M., Lehmann, M.F., Tortell P.D., 2008. Nitrogen and oxygen isotope
431 fractionation during dissimilatory nitrate reduction by denitrifying bacteria. *Limnol. Oceanogr.* 53,
432 2533 - 2545.

433 Higgins, M.B., Robinson, R.S., Husson, J.M., Carter, S.J., Pearson, A., 2012. Dominant eukaryotic
434 export production during ocean anoxic events reflects the importance of recycled NH_4^+. *PNAS*. 109,
435 2269 - 2274.

436 Hoch, M.P., Fogel, M.L., Kirchman, D.L., 1992. Isotope fractionation associated with ammonium
437 uptake by a marine bacterium. *Limnol*. *Oceanogr*. 37, 1447 - 1459.

438 Izon, G., Zerkle, A.L., Zhelezinskaia, I., Farquhar, J., Newton, R.J., Poulton, S.W., Eigenbrode, J.L.,
439 Claire, M.W., 2015. Multiple oscillations in Neoarchaean atmospheric chemistry. *E.P.S.L.* 431, 264 -
440 273.

441 Kendall, B., Reinhard, C.T., Lyons, T.W., Kaufman, A.J., Poulton, S.W., Anbar, A.D., 2010. Pervasive
442 oxygenation along late Archaean ocean margins. *Nat. Geosci*. 3, 647-652.

443 Knoll, A.H., Beukes, N.J., 2009. Introduction: Initial investigations of a Neoarchean shelf margin-basin
444 transition (Transvaal Supergroup, South Africa). *Precamb. Res*. 169, 1 - 14.

445 Luo, G., Shuhei Ono, S., Nicolas J. Beukes, N.J., David T. Wang, D.T., Shucheng Xie, S., Summons, R.E.
446 2016. Rapid oxygenation of Earth's atmosphere 2.33 billion years ago. *Science Advances* 13, 2,
447 e1600134

448 Luo, G., Junium, C.K., Izon, G., Ono, S., Beukes, N.J., Algeo, T.J., Cui, Y., Xie, S.,Summons, R.E., 2018.
449 Nitrogen fixation sustained productivity in the wake of the Palaeoproterozoic Great Oxygenation
450 Event. *Nat. Comms.* 9, 978.

451 McCready, R.G.L., Gould, W.D., Barendregt, R.W., 1983. Nitrogen isotope fractionation during the
452 reduction of NO_3^- to NH_4^+ by *Desulfovibrio* sp. *Canadian Jour. Microbiol*. 29, 231 - 234.

453 Miyano, T., Beukes, N.J., 1984. Phase relations of stilpnomelane, ferri-annite, and riebeckite in very
454 low grade metamorphosed iron formations. *Verh. Geol. Ver. S.-Afr*. 87, 111 - 124.

455 Möbius, J., Lahajnar, N., Emeis K-C., 2010. Diagenetic control of nitrogen isotope ratios in Holocene
456 sapropels and recent sediments from the Eastern Mediterranean Sea. *Biogeosci.* 7, 3901 - 3914.
457 Möbius, J., 2013. Isotope fractionation during nitrogen remineralization (ammonification):
458 implications for nitrogen isotope biogeochemistry. *Geochim. Cosmochim. Acta.* 105, 422-432.

459 Pavlov, A.A., Kasting, J.F., 2002. Mass-independent fractionation of sulfur isotopes in Archean
460 sediments: strong evidence for an anoxic Archean atmosphere. *Astrobiology*. 2, 27 - 41.

461 Peters, K.E., Sweeney, R.E., Kaplan, I.R., 1978. Correlation of carbon and nitrogen stable isotope
462 ratios in sedimentary organic matter. *Limn. Ocean*. 23, 598 - 604.

463 Polissar, P.J., Fulton, J.M., Junium, C.K., Courtney C. Turich, C.C., Freeman, K.H., 2009. Measurement
464 of ^{13}C and ^{15}N Isotopic Composition on Nanomolar Quantities of C and N. *Anal. Chem*. 81, 755 - 763.

465 Rau, G.H., Sullivan, W., Gordon, L.I., 1991. $\delta^{13}C$ and $\delta^{15}N$ variations in Weddell Sea particulate
466 organic matter. *Marine Chemistry*, 35, 355 – 369.

467 Sigman, D. M., Robinson, R., Knapp, A.N., van Geen, A., McCorkle, D. C., Brandes, J.A., Thunell, R.C.,
468 2003. Distinguishing between water column and sedimentary denitrification in the Santa Barbara
469 Basin using the stable isotopes of nitrate. *Geochem. Geophys. Geosys*. 4, 1040.

470 Sigman, D.M., Karsh, K.L., Casciotti, K.L., 2009. Ocean process tracers: Nitrogen isotopes in the
471 ocean. In: Steele, J.H., Turekian, K.K., (Eds.) Encyclopedia of Ocean Sciences. London: Academic
472 Press.

473 Stüeken, E.E., Kipp, M.A., Koehler, M.C., Buick, R., 2016. The evolution of Earth's biogeochemical
474 nitrogen cycle. *Earth Sci. Rev.,* 160, 220 - 239.

475 Stüeken, E.E., Zaloumis, J., Meixnerová, J., Buick, R., 2017. Differential metamorphic effects on
476 nitrogen isotopes in kerogen extracts and bulk rocks. *Geochim. Cosmochim. Acta.* 217, 80 - 94.

477 Sumner, D.Y., Grotzinger, J.P., 2004. Implications for Neoarchaean ocean chemistry from primary
478 carbonate mineralogy of the Campbellrand-Malmani Platform, South Africa. *Sedimentology*. 51,
479 1273 - 1299.

480 Sumner, D.Y., Beukes, N.J., 2006. Sequence stratigraphic development of the Neoarchean Transvaal
481 carbonate platform, Kapvaal Craton, South Africa. *S. Afr. J. Geol.* 109, 11 - 22.

482 Thomazo, C., Ader, M., Philippot, P., 2011. Extreme ^{15}N-enrichments in 2.72-Gyr-old sediments:
483 evidence for a turning point in the nitrogen cycle. *Geobiology*. 9, 107 - 120.

484 Walraven, F. and Martini, J., 1995. Zircon Pb-evaporation age determinations of the Oak Tree
485 Formation, Chuniesport Group, Transvaal Sequence: Implications for Transvaal-Griqualand West
486 basin correlations. *S Afr. J. of Geol.* 98, 58 - 67.

487 Walter M., Grotzinger J.P., Schopf J.W., 1992. Proterozoic stromatolites. In: Schopf J.W., Klein C.
488 (Eds.), The Proterozoic biosphere. A multidisciplinary study, Cambridge Univ. Press, Cambridge. 253 -
489 260.

490 Weber, T., Deutsch, C., 2014. Local versus basin-scale limitation of marine nitrogen fixation. *P.N.A.S.*
491 111, 8741 - 8746.

492 Yang, J., C. K. Junium, C.K., Grassineau, N.V., Nisbet, E.G., Izon, G., Mettam, C., Martin, A., Zerkle,
493 A.L., 2019. Ammonium availability in the Late Archaean nitrogen cycle. *Nat. Geosci*.
494 https://doi.org/10.1038/s41561-019-0371-1

495 Zerkle, A.L., Junium, C.K., Canfield, D.E., House, C.H., 2008. Production of ^{15}N-depleted biomass
496 during cyanobacterial N_2-fixation at high Fe concentrations. *Jour. Geophys. Res*. 113,
497 doi:10.1029/2007JG000651.

498 Zerkle, A.L., Claire, M.W., Domagal-Goldman, S.D., Farquhar, J., Poulton, S. W., 2012. A bistable
499 organic-rich atmosphere on the Neoarchaean Earth. *Nat. Geosci*. 5, 359 - 363.

500 Zerkle, A.L., Poulton, S.W., Newton, R.J., Mettam, C., Claire, M.W., Bekker, A., Junium, C.K., 2017.
501 Onset of the aerobic nitrogen cycle during the Great Oxidation Event. *Nature.* 542, 465 - 467.

502 Zhang, X., Sigman, D.M., Morel, F.M., Kraepiel, A.M., 2014. Nitrogen isotope fractionation by
503 alternative nitrogenases and past ocean anoxia. *P.N.A.S.* 111, 4782 - 4787.

504

505

Figure Legends

Fig 1. (A) Simplified stratigraphy of BH1-Sacha core (Altermann and Siegfried, 1997). (B) Simplified structure of Campbellrand-Malmani platform-top and ramp showing placement of BH1-Sacha core (Sumner and Beukes, 2006). (C) Position of BH1-Sacha drill site (star symbol) in South Africa (Sumner and Beukes, 2006). Dates in Figs. A and B are from a review in Sumner and Beukes (2009). More dates and references from correlative stratigraphy are presented in the supplementary information which confirm a date of 2588 to 2549 Ma for the Monteville Fm.

Fig. 2. Geochemical data for BH1-Sacha core. Nitrogen isotope data $\delta^{15}N_{org}$ (‰) are shown as black dots for silicates and triangles for carbonates, whilst $\delta^{15}N_{bulk}$ (‰) are shown as open pentagons). Carbonate abundance data (wt. %) are shown as dots. TOC (wt. %) and $\delta^{13}C_{org}$ **(‰)** data from this study are shown as dots, whilst data from Izon et al. (2015) are shown as open squares. Symbols for lithologies in core diagram as per Fig. 1A. Error bars for $\delta^{15}N_{org}$ reflect the combined standard deviation of N1 standards and triplicates of sample BH1-1963.6 using the equation: error bar = √ (

Fig. 3. Cross plots of geochemical data. Filled circles represent data from this study. Open squares include TOC and δ^{13}Corg data from Izon et al. (2015). Data shown: (A) TN_{org} and $\delta^{15}N_{org}$, (B) $\delta^{15}N_{org}$ and $\delta^{13}C_{org}$, (C) TOC/TN_{org} and $\delta^{15}N_{org}$ (D) TOC and $\delta^{13}C_{org}$, (E) TN_{bulk} and $\delta^{15}N_{bulk}$, (F) $\delta^{15}N_{bulk}$ and $\delta^{13}C_{org}$, (G) potassium and $\delta^{15}N_{bulk}$ and (H) TN_{bulk} and $\delta^{15}N_{bulk}$.

Fig. 4. Proposed model for facies-dependent nitrogen cycling at the ocean margin. This depositional setting is a well-defined marine marginal ramp and platform-top that could have reduced communication with the open ocean and led to somewhat isolated shallow **depositional settings.** Platform/ramp bathymetry and stromatolite assemblages are based upon idealised Proterozoic ramp and platform settings by Walter et al. (1992). Shown here are: **(A)** a shallow ramp top setting, representing the Schmidsdrift Subgroup and Monteville Fm; and **(B)** a lagoonal depositional setting, representing the Campbellrand Subgroup overlying the Monteville Fm. The proposed mechanisms include: **(1)** transport of diazotrophic biomass to the seafloor; **(2)** remineralization of OM to NH_4^+ and shoreward transport; **(3)** NH_4^+ assimilation, producing OM with -ve $\delta^{15}N$ values; **(4)** transport of a residual pool of NH_4^+ (possibly with +ve $\delta^{15}N$ values); **(5)** open ocean ammonium assimilation, producing OM with +ve $\delta^{15}N$ values; and, **(6)** potential for restricted open-marine influence but **(7)** potential for variability in communication as sea levels fluctuated.

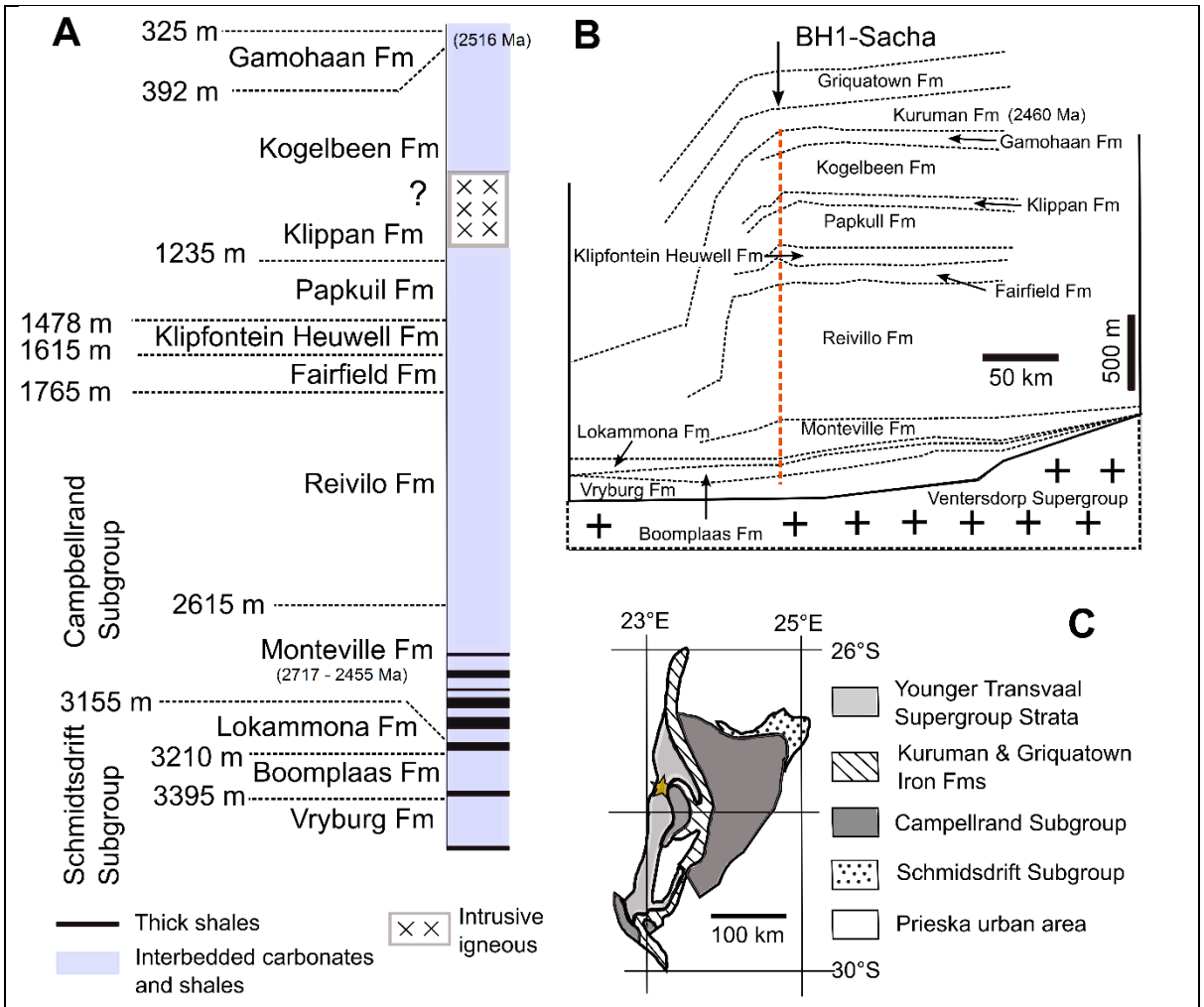

Fig 1. (A) Simplified stratigraphy of BH1-Sacha core (Altermann and Siegfried, 1997). (B) Simplified structure of Campbellrand-Malmani platform-top and ramp showing placement of BH1-Sacha core (Sumner and Beukes, 2006). (C) Position of BH1-Sacha drill site (star symbol) in South Africa (Sumner and Beukes, 2006). Dates in Figs. A and B are from a review in Sumner and Beukes (2009). More dates and references from correlative stratigraphy are presented in the supplementary information which confirm a date of 2588 to 2549Ma for the Monteville Fm.

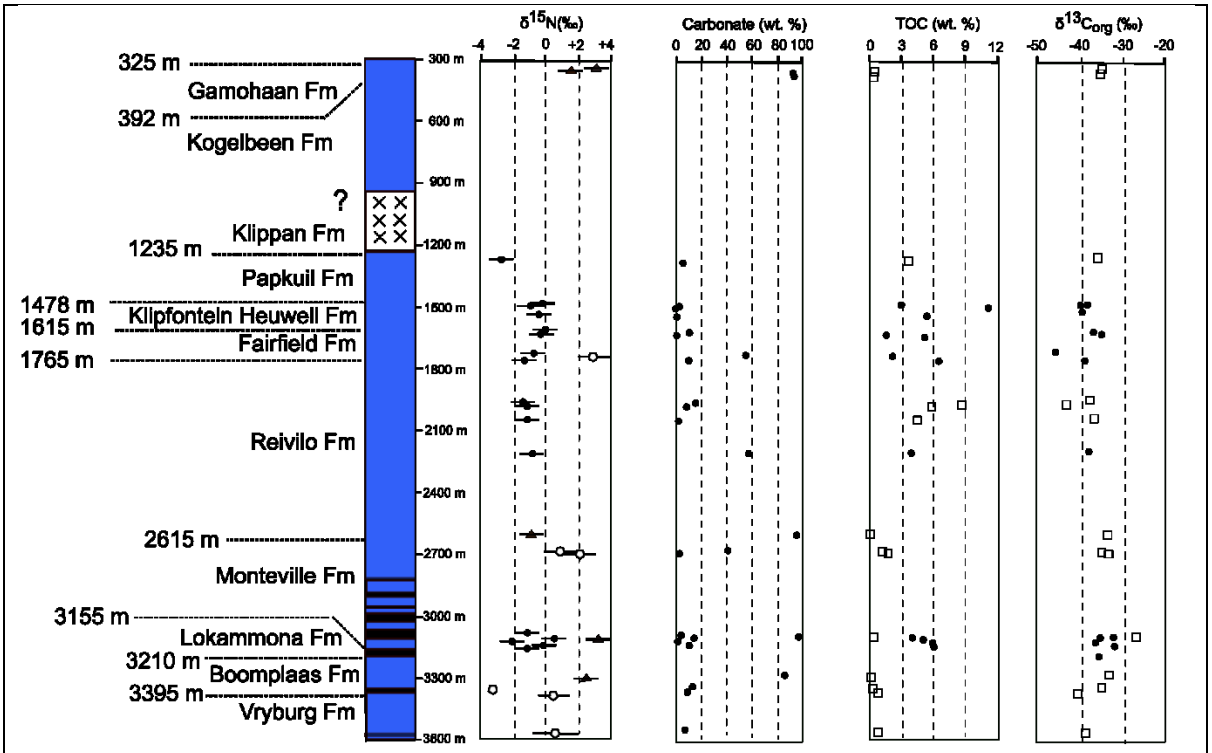

Fig. 2. Geochemical data for BH1-Sacha core. Nitrogen isotope data $\delta^{15}N_{org}$ (‰) are shown as black dots for silicates and triangles for carbonates, whilst $\delta^{15}N_{bulk}$ (‰) are shown as open pentagons). Carbonate abundance data (wt. %) are shown as dots. TOC (wt. %) and $\delta^{13}C_{org}$ **(‰)** data from this study are shown as dots, whilst data from Izon et al. (2015) are shown as open squares. Symbols for lithologies in core diagram as per Fig. 1A. Error bars for $\delta^{15}N_{org}$ reflect the combined standard deviation of N1 standards and triplicates of sample BH1-1963.6 using the equation: error bar = √ (error of standards^2 + largest error of corrected sample^2)]. Error bars are thus ±0.7‰. Error bars for $\delta^{15}N_{bulk}$ reflect the combined standard deviation of standards and the intercept errors of keeling plots for each sample triplicate using the same formula. These are shown in the supplementary tables.

543

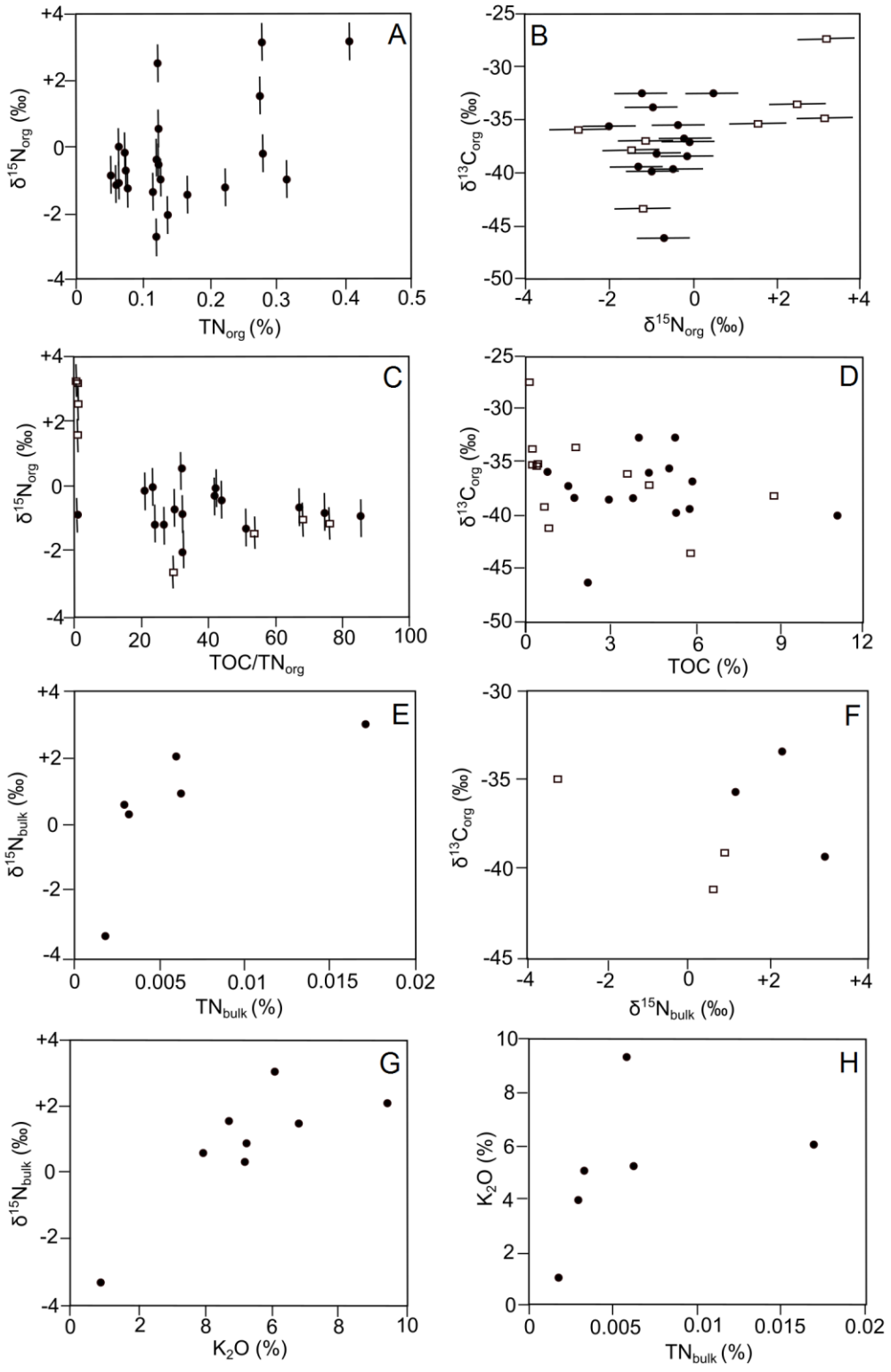

Fig. 3. Cross plots of geochemical data. Filled circles represent data from this study. Open squares include TOC and δ^{13}Corg data from Izon et al. (2015). Data shown: (A) TN_{org} and $\delta^{15}N_{org}$, (B) $\delta^{15}N_{org}$ and $\delta^{13}C_{org}$, (C) TOC/TN_{org} and $\delta^{15}N_{org}$ (D) TOC and $\delta^{13}C_{org}$, (E) TN_{bulk} and $\delta^{15}N_{bulk}$, (F) $\delta^{15}N_{bulk}$ and $\delta^{13}C_{org}$, (G) potassium and $\delta^{15}N_{bulk}$ and (H) TN_{bulk} and $\delta^{15}N_{bulk}$.

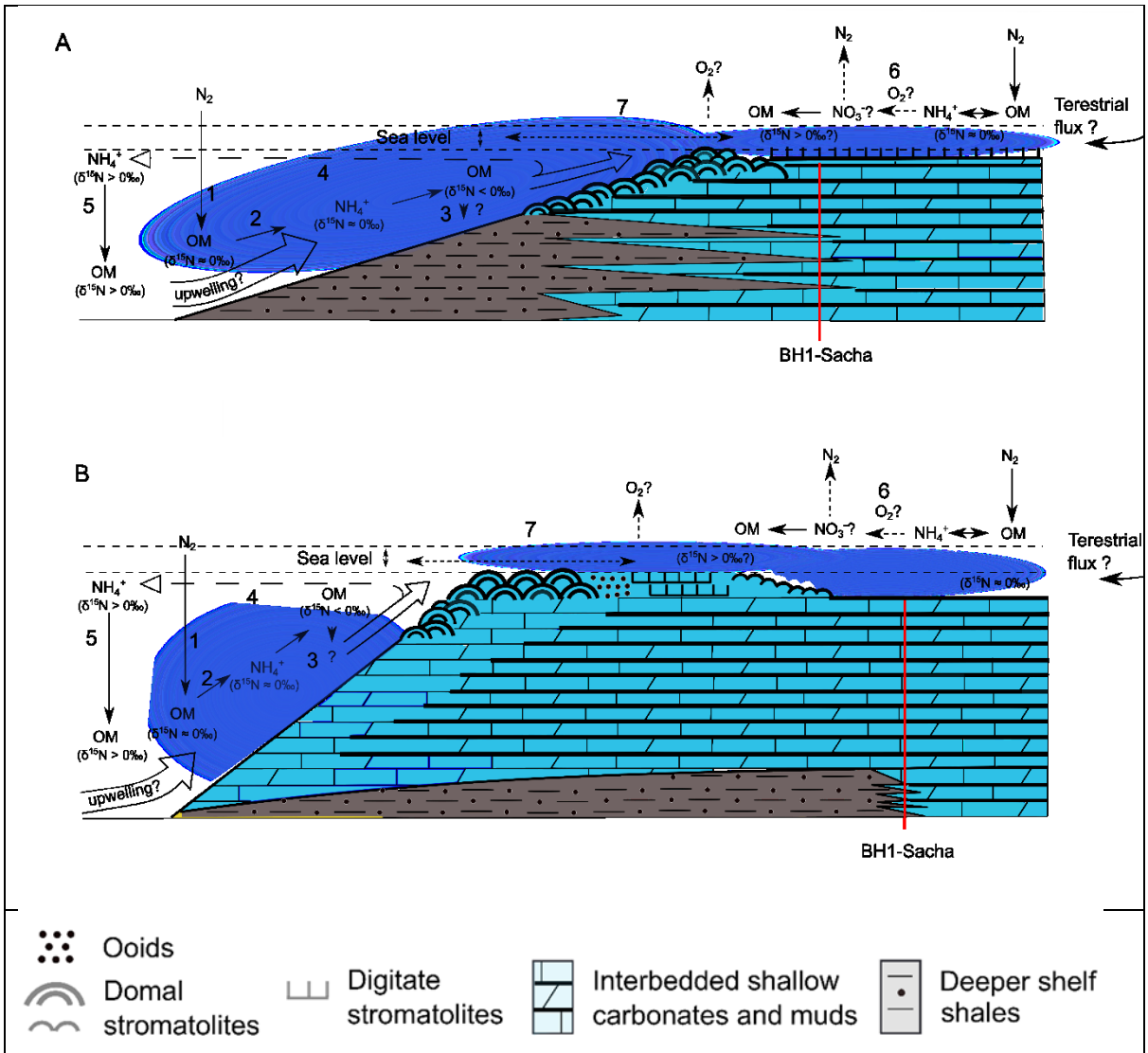

Fig. 4. Proposed model for facies-dependent nitrogen cycling at the ocean margin. This depositional setting is a well-defined marine marginal ramp and platform-top that could have reduced communication with the open ocean and led to somewhat isolated shallow depositional settings. Platform/ramp bathymetry and stromatolite assemblages are based upon idealised Proterozoic ramp and platform settings by Walter et al. (1992). Shown here are: **(A)** a shallow ramp top setting, representing the Schmidsdrift Subgroup and Monteville Fm; and **(B)** a lagoonal depositional setting, representing the Campbellrand Subgroup overlying the Monteville Fm. The proposed mechanisms include: **(1)** transport of diazotrophic biomass to the seafloor; **(2)** remineralization of OM to NH_4^+ and shoreward transport; **(3)** NH_4^+ assimilation, producing OM with -ve $\delta^{15}N$ values; **(4)** transport of a residual pool of NH_4^+ (possibly with +ve $\delta^{15}N$ values); **(5)** open ocean ammonium assimilation, producing OM with +ve $\delta^{15}N$ values; and, **(6)** potential for restricted open-marine influence but **(7)** potential for variability in communication as sea levels fluctuated.